Available online at www.sciencedirect.com
SCIENCE DIRECT®
Applied Catalysis A: General 242 (2003) 403–416
APPLIED CATALYSIS A: GENERAL
www.elsevier.com/locate/apcata

Reduction behaviour of Fe/ZrO_2 and $Fe/K/ZrO_2$ Fischer–Tropsch catalysts

F.R. van den Berg [a], M.W.J. Crajé [b], A.M. van der Kraan [b,*], J.W. Geus [a]

[a] *Department of Inorganic Chemistry, Debije Institute, Utrecht University, P.O. Box 80083, TB Utrecht 3508, The Netherlands*
[b] *Interfacultair Reactor Instituut, Delft University of Technology, Mekelweg 15, JB Delft 2629, The Netherlands*

Received 14 June 2002; received in revised form 30 September 2002; accepted 30 September 2002

Abstract

The reduction behaviour (the activation process) of two iron-based Fischer–Tropsch catalysts viz. an unpromoted and a potassium-promoted zirconia-supported iron catalyst is investigated. The initial dispersion of both catalysts is very high. To establish the nature of the iron species under hydrogen atmosphere, experiments were performed at ambient pressure. It is demonstrated for both catalysts that during reduction the carbon originating from the citrate complex used in the preparation procedure is not completely removed, whereby the largest amount of the carbon species is encountered on the potassium-promoted catalyst. During reduction at ambient pressure this residual carbon reacts with metallic iron and forms cementite (θ-Fe_3C). The iron oxide of the potassium-promoted catalyst turns out to reduce more easily than the oxide of the unpromoted catalyst. Upon formation of divalent iron, this divalent species readily reacts with the support to give a stable mixed oxide. This mixed oxide is suggested to be a prerequisite in maintaining a high dispersion of the metallic iron particles. Based on the analyses presented here, a reduction model is proposed.

Keywords: Fischer–Tropsch catalysts; Reduction model; Iron oxide; Mössbauer spectroscopy

1. Introduction

The conversion of synthesis gas or syngas, a mixture of CO and H_2, into mainly hydrocarbons is known as the Fischer–Tropsch (FT) synthesis. This synthesis is named after Franz Fischer and Hans Tropsch, who published the production of hydrocarbons over cobalt catalysts already in the early 20's [1–3]. To produce liquid transport fuels from coal, which is abundantly available in Germany in contrast to crude oil, much research was preformed on the FT process before World War II. Just before the beginning of World War II it was found that at pressures of 15–20 bar iron can be employed as a catalyst for the FT process.

Nowadays, Sasol in South Africa is operating Fischer–Tropsch plants based on the application of supported iron-based catalysts. The synthesis gas for the FT units is produced in large Lurgi gasifiers, in which the coal is gasified in a moving bed by reaction with steam and oxygen.

Since the FT synthesis is rather expensive the synthesis can only compete with the oil refineries if the oil price is over $ 16 per barrel. Nevertheless nowadays, the production of liquid hydrocarbons by FT synthesis whereby methane is used as starting material instead of coal is considered, the so-called gas-to-liquid (GTL process). This process is a way to exploit remote gas fields as well as to limit the emission of carbon dioxide by flaring of methane being released during the production of crude oil. The synthesis gas is produced

* Corresponding author.

0926-860X/02/$ – see front matter
PII: S0926-860X(02)00532-X

by partial oxidation or catalytic partial oxidation of methane with pure oxygen to carbon monoxide and hydrogen.

As olefins are presently one of the most important feedstocks for the production of chemicals, the direct production of light olefins from syngas is very attractive. The ability to produce light olefins is heavily dependent on the catalyst design, for example, on the active metal, the support, the dispersion and the promoter employed.

Iron is chosen as the active metal for its ability to dissociatively adsorb CO faster than H_2, which enhances the olefinic selectivity. Iron is able to produce unsaturated hydrocarbons better than any other metal. However, iron also deactivates more easily due to surface segregation of graphitic layers. Analogous to very small nickel particles, the growth of graphite layers on very small iron particles is enormously reduced [4,5]. Filamentous carbon is only observed with metal particles of a size exceeding about 5 nm [6,7]. In order to increase the stability of small particles, the required high dispersion should be stabilised by the support due to a suitable metal-support interaction, which only partially involves the active iron particles and does not deactivate the active species. It has further been reported that potassium oxide raises the selectivity towards olefins. Therefore, potassium has been added as a promoter to the catalyst and, additionally, to suppress the formation of carbon nanowires. The support should not interact with the employed K-promoter to avoid diminishing its promoting effect. Zirconia is known not to pronouncedly interact with alkali metals, while it has been suggested that zirconia interacts with iron [8–11]. For this reason, the support of choice in the present study is zirconia (ZrO_2). Sofar, only catalytic systems with bimodal distributions of sizes of iron particles have been described and it is further reported that ZrO_2 changes the catalytic properties of the iron particles [8–11]. However, these properties have not been extensively studied. To achieve iron particles of a uniform small size evenly distributed over a zirconia support low loadings of iron will be employed in the present study.

Recently, we reported the preparation of the highly dispersed oxidic precursors of the unpromoted Fe/ZrO_2 and the potassium-promoted Fe/K/ZrO_2 catalysts using the incipient wetness impregnation and an organic chelating citrate [12]. The aim of the present study is to elucidate the reduction behaviour (the activation process) of the unpromoted (Fe/ZrO_2) and the potassium-promoted (Fe/K/ZrO_2) zirconia-supported iron catalysts at ambient hydrogen pressure in more details than already reported in the literature [9–11, 13–16].

The reduction of bulk hematite (α-Fe_2O_3) proceeds via magnetite (Fe_3O_4) and woestite (FeO) to metallic iron [17,18]. However, the formation of FeO is not observed, because woestite is metastable below 843 K [17–19] at which temperature disproportionation into Fe_3O_4 and Fe proceeds.

With supported iron catalysts the purely divalent state of iron can be stabilised well below the critical temperature by interaction with the support due to formation of mixed oxides. For iron catalysts supported on Al_2O_3 and SiO_2 the formation of ferrous aluminates and silicates has been reported [18,20–24]. Wielers et al. [21] observed the formation of a silicate layer during reduction of trivalent iron indicating that, as soon as divalent iron is formed, iron migrates into the support. Also with TiO_2 and MgO supports mixed oxides are mentioned to account for the intimate contact between the precursor metal oxide and the support resulting in a lower reducibility of the iron oxide [13–15].

It will be shown that water plays an essential role in the reduction of the zirconia-supported iron oxide catalysts. Furthermore, it is argued that a mixed oxide of iron and the ZrO_2-support is possibly present. Finally, it will be demonstrated that upon formation of metallic iron as a result of the activation process the dispersion of the iron species drops rapidly. In addition, our experimental results indicate beyond doubt that the freshly calcined catalysts contain an appreciable amount of carbon originating from the initially impregnated citrate precursor as reported before [12]. The potassium oxide promoter appears to affect strongly the mobility of carbon.

2. Experimental

2.1. Catalyst preparation

The catalysts were prepared by means of incipient wetness impregnation. The pre-shaped support material used was zirconia (Norton XZ16075). The

pore volume of the zirconia is 0.28 ml/g and the BET surface area is 49 m^2/g. Ammonium iron(III) citrate (Merck, 28% Fe) was employed as precursor to obtain a calculated iron loading of 2.5 wt.%. The potassium-promoted catalyst was prepared by co-impregnation of ammonium iron(III) citrate and potassium carbonate; an atomic ratio Fe/K of 1 was applied. For Mössbauer measurements, a citrate complex enriched with the ^{57}Fe isotope was prepared in order to shorten the measuring times. After impregnation the loaded support was dried at 350 K within flowing air, and subsequently calcined at 723 K for 2 h (heating rates were 5 K/min). The advantage of the citrate complex as precursor and details of the characterisation of the freshly prepared Fe/ZrO_2 and Fe/K/ZrO_2 catalysts are presented in [12].

2.2. Mössbauer absorption spectroscopy (MAS)

The experiments at ambient hydrogen pressure (1 bar) were executed using an in situ Mössbauer reactor described in more details in [25]. The catalysts (about 100 mg) were reduced in a hydrogen atmosphere at temperatures from 300 up to 823 K and measured in situ at the applied reduction temperature. As the catalyst may change during these measurements, in some cases the reduced catalyst is subsequently also measured at room temperature without changing the hydrogen gaseous environment.

Mössbauer measurements were carried out in a constant acceleration mode using a ^{57}Co in Rh source. Isomer shifts are reported relative to the NBS standard sodium nitroprusside ($Na_2Fe(CN)_5NO.2H_2O$). Magnetic hyperfine fields (H_{eff}) were calibrated with the 515 kOe field of α-Fe_2O_3 at room temperature. The Mössbauer parameters were determined by fitting the spectra with subspectra consisting of Lorentzian-shaped lines (Γ is the line width) using a non-linear iterative minimisation routine. The accuracy for the isomer shift (I.S.) is ±0.03 mm/s, for the electric quadrupole splitting (Q.S.) ±0.05 mm/s, for the hyperfine field (H_{eff}) ±2 kOe and for the spectral contribution (S.C.) 5%.

2.3. Thermomagnetic analysis (TMA)

The catalysts (about 150 mg) were pretreated in a quartz flow reactor of a diameter of 10 mm operated at atmospheric pressure. Magnetisation measurements were performed using a modification of the Weiss-extraction method [26]. With this technique it is possible to monitor the magnetisation of the iron phase under reaction conditions. Fig. 1 shows a schematic representation of the apparatus. Experiments were carried out at a magnetic field strength of 7 kOe.

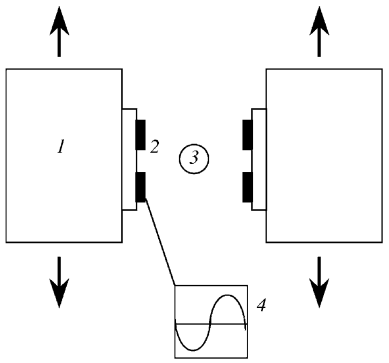

Fig. 1. Schematic representation of equipment for magnetic measurements. Horizontal cross-section: (1) moving electromagnet; (2) Helmholz sensing coils; (3) reactor and catalyst; (4) integrator.

All samples were treated in a 50 ml/min 10% H_2/He (v/v) gas flow at temperatures from 298 K up to a temperature of 823 K. The temperature was raised in steps of 10 K and the magnetisation was determined at every temperature. Subsequently the magnetisation was measured at temperatures decreasing in steps of 10 K to room temperature. The magnetisation was normalised taking into account the total mass of iron in the measured sample.

2.4. Temperature-programmed reduction (TPR)

The temperature-programmed reduction experiments were performed in a downstream quartz plug-flow reactor (ϕ = 8 mm) at atmospheric pressure. The catalyst (about 50 mg) was reduced in a 5% H_2/Ar (v/v) flow of 20 ml/min, while the temperature was increased from room temperature to 1373 K at a linear heating rate of 10 K/min. The water formed was frozen in a cold (aceton–carbon dioxide) trap. The hydrogen consumption was monitored using a hot wire detector.

3. Results

3.1. Reduction of Fe/ZrO_2 studied by MAS

In [12] it is shown that the freshly calcined catalyst contains exclusively trivalent iron (I.S. = 0.60 mm/s, Q.S. = 0.99 mm/s at 300 K). Presently, in situ Mössbauer measurements during reduction treatments at different temperatures and a hydrogen pressure of 1 bar are described.

As can be seen in Table 1 and Fig. 2(a), reduction at 573 K results in the appearance of two spectral components. From the two deduced I.S.—values at 573 K, which are both much larger than 0.60 mm/s (the I.S.—value of the Fe^{3+} in the fresh calcined catalyst precursor at 300 K), it follows that both spectral components can be assigned to divalent iron species. The two divalent iron species are different in nature considering the different isomer shift and quadrupole splitting.

During reduction at 623 K three different contributions are observed in the spectrum (see Fig. 2(b) and Table 1). Two contributions are attributed to divalent iron species similar to the species found at 573 K. The third spectral component with I.S. = 0.26 mm/s and Q.S. = 0.48 mm/s is assigned to θ-Fe_3C (cementite) above its magnetic ordering temperature of 485 K [27]. This assignment is confirmed by the magnetically split component (H_{eff} = 205 kOe) in the spectrum measured at 300 K (see Section 3.4). The formation of θ-Fe_3C is without doubt due to the presence of carbon in the catalyst which remained due to incomplete decomposition of the citrate precursor upon calcination at 723 K [12]. As the atomic ratio of iron-to-carbon in the calcined Fe/ZrO_2 catalyst is determined by thermogravimetry to be 4.5/5.3 [12], the amount of carbon is more than sufficient to accommodate the cementite formation to the extent observed.

During the reduction treatment at the even more elevated temperature of 673 K (Table 1 and Fig. 2(c)) a magnetically split spectral component with H_{eff} = 293 kOe is observed. This contribution is due to the appearance of metallic iron (Fe^0) in the catalyst sample measured at 673 K. Next to this metallic contribution the spectrum comprises the two earlier observed doublets of Fe^{2+} and the one ascribed to θ-Fe_3C.

Raising the reduction temperature to 723 K leads to a spectrum displaying the same four spectral contributions as after reduction at 673 K (see Fig. 2(d) and Table 1). The higher reduction temperature of 723 K increases the contribution of metallic iron to the spectrum to about 30%. The spectral contribution of θ-Fe_3C does not significantly change as compared to

Table 1
Mössbauer parameters of 2.5 wt.% Fe/ZrO_2 deduced from the spectra measured during reduction at 573, 623, 673, 723, 773 and 823 K

T (K)	I.S. (mm/s)	Q.S. (mm/s)	H_{eff} (kOe)	Γ (mm/s)	S.C. (%)	Compound
573 (0–22 h)	0.75	0.62		0.51	27	Fe^{2+}
	0.99	1.50		0.58	73	Fe^{2+}
623 (0–21 h)	0.27	0.50		0.24	7	Fe_3C
	1.01	1.29		0.54	63	Fe^{2+}
	0.68	0.95		0.49	30	Fe^{2+}
673 (0–22 h)	0.02	0.00	293	0.23	6	Fe^0
	0.22	0.46		0.33	19	Fe_3C
	0.97	1.23		0.55	49	Fe^{2+}
	0.68	0.88		0.53	26	Fe^{2+}
723 (0–20 h)	−0.02	0.00	288	0.27	27	Fe^0
	0.19	0.45		0.38	19	Fe_3C
	0.92	1.21		0.51	28	Fe^{2+}
	0.72	0.81		0.57	26	Fe^{2+}
773 (0–29 h)	−0.05	0.00	279	0.29	70	Fe^0
	0.74	0.83		0.72	30	Fe^{2+}
823 (0–21 h)	−0.08	0.00	268	0.29	87	Fe^0
	0.76	0.88		0.97	13	Fe^{2+}

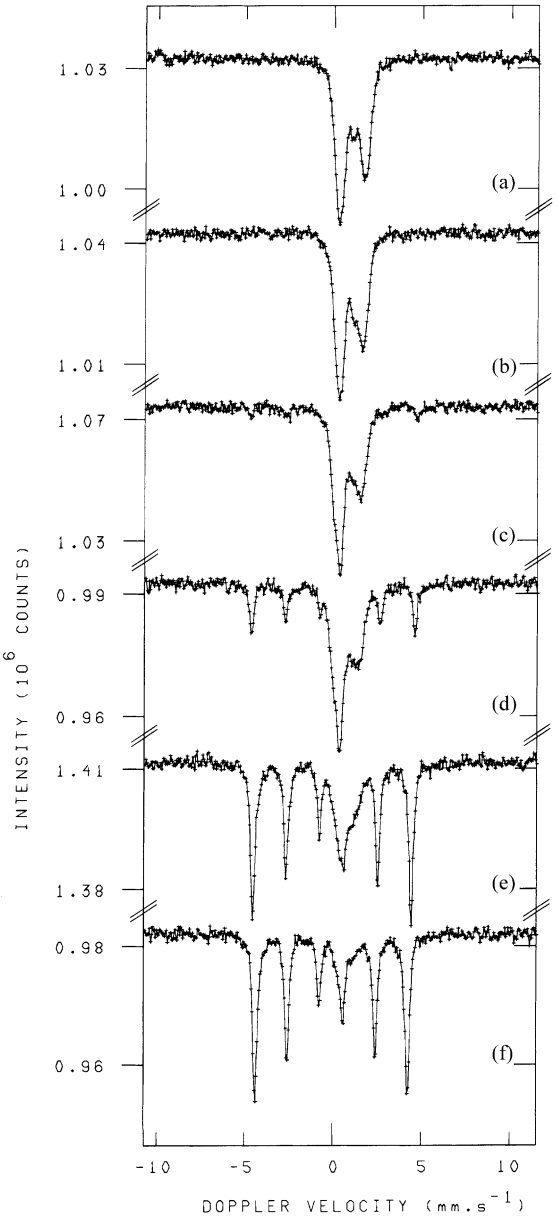

Fig. 2. Mössbauer spectra of 2.5 wt.% Fe/ZrO_2 measured during reduction at: (a) 573 K; (b) 623 K; (c) 673 K; (d) 723 K; (e) 773 K and (f) 823 K.

the contribution found after the previous reduction step at 673 K. The fact that the contribution of θ-Fe_3C does not increase further implies that apparently no carbon is left nearby to react with metallic iron; a substantial fraction of the carbon left behind by the decomposed citrate precursor is hydrogenated to methane or does not contact the iron particles. As at a reduction temperature of 773 K or above, the contribution of θ-Fe_3C to the spectrum has disappeared (see Fig. 2(e,f) and Table 1), it can be concluded that the cementite in the sample is completely hydrogenated.

3.2. Reduction of Fe/ZrO_2 studied by TMA

Fig. 3 represents a thermomagnetic profile wherein the reduction in flowing hydrogen of the zirconia-supported iron-based catalyst (Fe/ZrO_2) is monitored.

With a vibrating sample magnetic measuring technique (VSM) it was established that any ferromagnetism is absent in the freshly calcined catalyst, in agreement with the results obtained using Mössbauer spectroscopy [12]. Hence, the measured thermomagnetic profile of the fresh catalyst has been corrected for the observed offset exhibited by the measuring device. An increase in magnetisation is observed at about 568 K, the temperature being referred to as the onset temperature T_{onset}. Above T_{onset} two regions, each region showing a different slope, are encountered indicating different reduction rates. The increase in magnetisation is indicating the formation of ferromagnetic Fe^0 species. With Mössbauer spectroscopy two non-magnetic Fe^{2+} species have been observed during reduction at 573 K (see Fig. 2 and Table 1). These species can be ascribed to a surface species $Fe(I)^{2+}$ and a species $Fe(II)^{2+}$ which is part of a mixed oxide with the support. It is very likely that during the reduction treatment first the surface species $Fe(I)^{2+}$ will be reduced to Fe^0. In a subsequent step reduction of species $Fe(II)^{2+}$ will proceed at a much lower rate as the support possibly stabilizes this iron containing mixed oxide species. In this step the 'mixed' Fe^{2+} first migrates to the surface (becoming $Fe(I)^{2+}$ and, subsequently, is converted to metallic iron Fe^0. The inflection point at which both reduction regimes meet can provide an indication of the amount of $Fe(I)^{2+}$ and, complementary, the amount of $Fe(II)^{2+}$, since reduction to Fe^{2+} proceeds completely prior to the formation of metallic iron as shown by the Mössbauer spectra (see Fig. 2 and Table 1).

Mössbauer experiments have shown that the reduction eventually leads to metallic iron (Fe^0) which is established by the ferromagnetic profile measured during the decrease in temperature after having

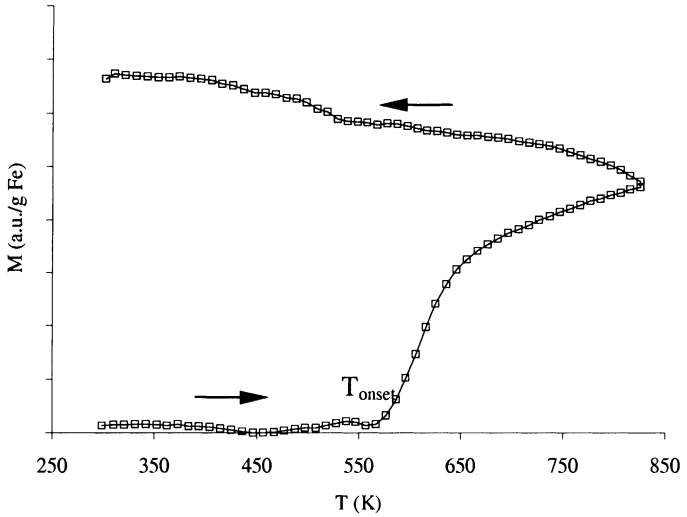

Fig. 3. Thermomagnetic profile of 2.5 wt.% Fe/ZrO_2.

reached the maximum applied temperature. Extrapolation of this branch of the magnetisation curve to higher temperatures shows that the Curie temperature of the involved species is well above the maximum applied reduction temperature (823 K). Since only α-Fe has such a high Curie temperature, viz. T_C is 1043 K, reduction to metallic iron is apparent.

Fig. 3 shows that upon cooling an additional increase in magnetisation is exhibited at about 520 K. The Curie temperature estimated from the inflection point of the curve measured at decreasing temperature [26] is about 490 K, which is, considering that Mössbauer results show the formation of cementite (θ-Fe_3C) during reduction, attributable to θ-Fe_3C having a Curie temperature of 485 K [27]. The θ-Fe_3C is formed out of α-Fe during the reduction. As the reduction to α-Fe starts at a temperature above the Curie temperature of θ-Fe_3C, the cementite was invisible in the increasing temperature branch of the TMA profile.

Additionally, from the observed TMA profile, it is possible to calculate the (molar) contribution of the carbide species. The magnetisation observed at room temperature is a superposition of the magnetisation of cementite and zerovalent iron. The magnetic contribution of the iron carbide is determined as indicated in Fig. 4.

In the thermomagnetic experiment, the magnetisation is provided in arbitrary units. But, the ratio of the magnetisation due to Fe^0 and due to θ-Fe_3C is a direct measure for their contributions in the catalyst. This ratio is calculated to be $(0.4/6.4) = 0.06$. For determination of the molar contribution of the carbide, the lower saturation magnetisation of the carbide must be taken into account. The relative saturation magnetisation (i.e. the ratio of the saturation magnetisation of metallic iron and the carbide) is estimated to be the ratio of the hyperfine splittings of Fe^0 (331 kOe) and θ-Fe_3C (208 kOe) observed with Mössbauer

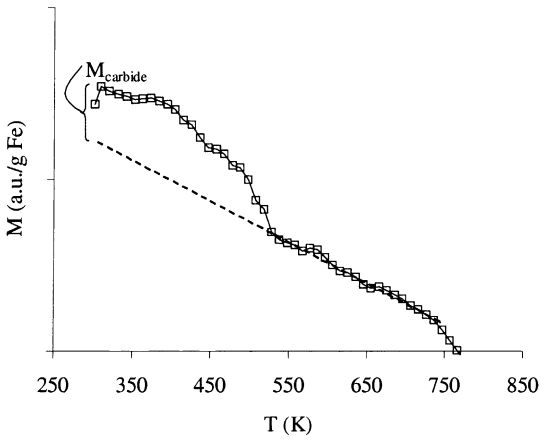

Fig. 4. Determination of the magnetic contribution of θ-Fe_3C in the TMA-profile. This Figure is a magnification of part of Fig. 3.

spectroscopy [28]. The thus calculated value for the amount of cementite becomes about 10% of the zerovalent iron present in the catalyst. Assuming that the reduction is complete (100%) this value of 10% is in good agreement with the Mössbauer results.

3.3. Reduction of Fe/ZrO_2 studied by TPR

The TPR-profile is shown in Fig. 5. Two regions with large H_2 consumption are distinguished, which are separated by a low hydrogen consumption at about 800 K.

After the first region, the degree of reduction was roughly estimated to be around 33%, indicating the reduction from Fe^{3+} to Fe^{2+}. The measured profile of this region consists of a large peak at about 620 K with a shoulder at about 710 K. The calculated area of the shoulder is much smaller than that of the first peak. As the ratio of the hydrogen consumption upon reduction of Fe_2O_3 to Fe_3O_4 and the hydrogen consumption upon further reduction to FeO is 1:2, it follows that the reduction does not proceed via a magnetite phase. This result is in agreement with those obtained by Mössbauer spectroscopy.

The degree of reduction at a certain temperature as found by the TPR experiment remained below the values deduced from the in situ Mössbauer absorption experiments and thermomagnetic analysis. This is most probably due to the strong influence of the hydrogen partial pressure on the reduction behavior and the applied relative high heating rate of 10 K/min in the TPR experiment. Boot et al. [8,16] reported that the use of a higher hydrogen partial pressure caused the Fe/ZrO_2 catalyst to be reduced completely at much lower temperature, while the use of the lower H_2 partial pressure showed better resolution of the different reduction peaks. These effects were explained by Wimmers et al. [29] by combining thermodynamic and kinetic effects: a higher pH_2/pH_2O ratio caused the reduction to be completed at lower temperatures and the higher H_2 concentration itself increased the overlap of reduction peaks.

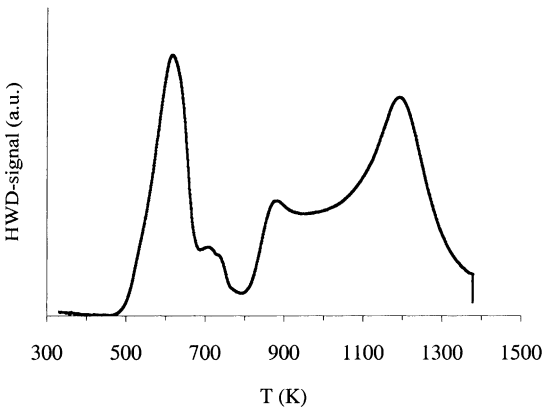

Fig. 5. Temperature-programmed reduction profile of 2.5 wt.% Fe/ZrO_2.

The degree of reduction is calculated to be 100% after the completion of the second region. This region consists of two maxima, most probably indicating the presence of two different Fe^{2+} species reacting to Fe^0.

3.4. Re-oxidation in H_2 of reduced Fe/ZrO_2

The MAS measurements of the reduction behaviour of the Fe/ZrO_2 catalyst were performed in situ at the reduction temperatures. As however, the catalyst may have changed *during* these measurements, the finally obtained reduced catalyst was cooled to room temperature maintaining it in the reducing H_2-atmosphere and subsequently measured at 300 K. As a first result, the spectral composition significantly changed. Re-oxidation of the Fe/ZrO_2 catalyst reduced at 573 K was observed at room temperature and it turned out that this re-oxidation proceeded with time, excluding the possibility that the change in spectral composition is due to a difference in Debije-temperature of the Fe^{2+} and Fe^{3+} species. Finally, a large amount of Fe^{3+} was observed (83%), whereas at 573 K all trivalent iron had been reduced to Fe^{2+}. Apparently, even in a hydrogen atmosphere re-oxidation of Fe^{2+} occurs during cooling to and at room temperature. It must be noted that the re-oxidation process took place both in static and flowing hydrogen, hence, excluding the possibility of oxygen leakage.

This re-oxidation behaviour was unexpected and therefore, it is studied in more detail. In Fig. 6, the spectra measured during a period of about 24 h at room temperature after reduction at 573, 623, 673, 723, 773 and 823 K, respectively, are presented. Comparing the measured spectra of Fig. 2 with those of Fig. 6, it follows that also the catalysts reduced at 623, 673 and 723 K, respectively, re-oxidise during or after decreasing the temperature to room temperature,

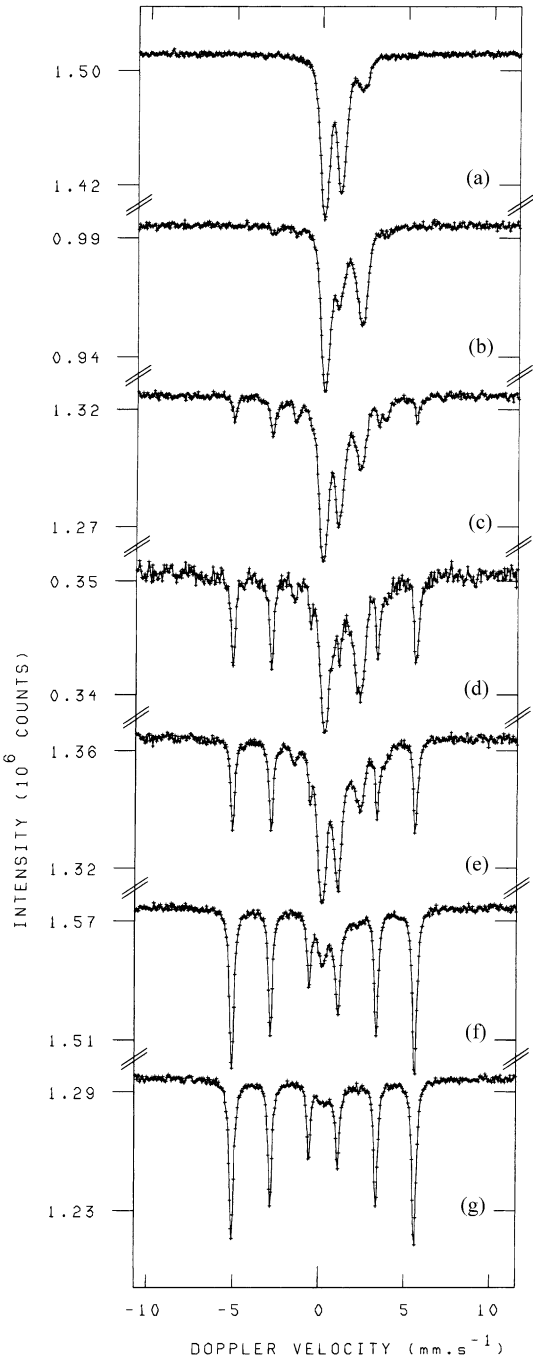

Fig. 6. Mössbauer spectra at room temperature of 2.5 wt.% Fe/ZrO_2 measured after reduction at: (a) 573 K (0–32 h); (b) 623 K (0–20 h); (c) 673 K; (0–26 h); (d) 723 K (0–6 h); (e) 723 K (0–26 h); (f) 773 K (0–29 h) and (g) 823 K (0–21 h).

similar to the one reduced at 573 K. The Mössbauer parameters determined from the analyses are given in Table 2. It turns out that in the spectra at 300 K of the catalysts reduced at 623, 673 and 723 K, respectively, besides the expected spectral component of metallic Fe^0 ($H_{eff} \sim 330$ kOe), an additional magnetic component is present ($H_{eff} \sim 208$ kOe). This spectral component is assigned to θ-Fe_3C [28] and is due to the presence of carbon in the catalyst which remains after decomposition of the citrate precursor upon calcination at 723 K [12]. To show the instability of the reduced samples at room temperature in the H_2 atmosphere, also a measurement during the first 6 h after cooling to room temperature is included in Fig. 6 for reason of comparison.

In addition, the spectral parameters computed from measurements taken during the first 9, 8 or 6 h after cooling down and after a more prolonged period of time at room temperature are presented in Table 2. From the changes in spectral composition with time it follows that the re-oxidation progresses at room temperature.

From Table 2 it is evident that only the Fe^{2+} species are partly converted to Fe^{3+} and that the ferromagnetic phases (metallic Fe^0 and θ-Fe_3C) do not change with time.

3.5. *Reduction of potassium-promoted Fe/K/ZrO_2 studied by MAS*

Also the behaviour of $Fe/K/ZrO_2$ during reduction is followed in situ with Mössbauer spectroscopy. Since the measurements on the Fe/ZrO_2 catalyst have well established the re-oxidation at room temperature of the Fe^{2+} species produced during the reduction, only spectra are measured at the applied reduction temperature during the treatment. Fig. 7 shows a compilation of the spectra measured during the reduction at 473, 573, 623, and 653 K. In Table 3 the Mössbauer parameters calculated from all the measured spectra are given.

Reduction at 373 and 473 K does not affect the spectrum as compared to the initial spectrum at 300 K. The parameters calculated from the spectra point to the presence of exactly the same Fe^{3+} species as observed in Fe/ZrO_2.

During the reduction at 573 K three spectral contributions appear which are different from the Fe^{3+}

Table 2
Mössbauer parameters of 2.5 wt.% Fe/ZrO_2 calculated from spectra measured at 300K after the reduction at 573, 623, 673, 723, 773 and 823 K

$T_{(meas)}$ (K)	$T_{(red)}$ (K)	I.S. (mm/s)	Q.S. (mm/s)	H_{eff} (kOe)	Γ (mm/s)	S.C. (%)	Compound
300 (0–32 h)	573	1.23	2.67		0.28	7	Fe^{2+}
		1.26	1.96		0.35	10	Fe^{2+}
		0.60	0.99		0.58	83	Fe^{3+}
300 (0–9 h)	623	0.47		205	0.29	3	Fe_3C
		1.31	2.29		0.44	39	Fe^{2+}
		1.25	1.68		0.59	48	Fe^{2+}
		0.58	0.90		0.53	10	Fe^{3+}
300 (0–20 h)	623	0.47		205	0.24	3	Fe_3C
		1.31	2.41		0.39	22	Fe^{2+}
		1.27	1.84		0.57	40	Fe^{2+}
		0.58	0.91		0.59	35	Fe^{3+}
300 (0–8 h)	673	0.27	0.00	330	0.26	10	Fe^0
		0.47		204	0.39	14	Fe_3C
		1.31	2.38		0.35	16	Fe^{2+}
		1.26	1.78		0.60	50	Fe^{2+}
		0.58	0.90		0.72	10	Fe^{3+}
300 (0–26 h)	673	0.26	0.00	331	0.27	10	Fe^0
		0.47		205	0.38	14	Fe_3C
		1.24	2.54		0.30	6	Fe^{2+}
		1.21	1.95		0.55	20	Fe^{2+}
		0.61	0.94		0.62	50	Fe^{3+}
300 (0–6 h)	723	0.26	0.00	332	0.28	34	Fe^0
		0.47		210	0.35	10	Fe_3C
		1.34	2.31		0.38	13	Fe^{2+}
		1.25	1.76		0.63	35	Fe^{2+}
		0.58	0.90		0.71	8	Fe^{3+}
300 (0–26 h)	723	0.26	0.00	331	0.27	31	Fe^0
		0.47		208	0.40	11	Fe_3C
		1.28	2.03		0.67	21	Fe^{2+}
		0.67	1.34		0.50	6	Fe^{2+}
		0.58	0.90		0.57	31	Fe^{3+}
300 (0–29 h)	773	0.26	0.00	331	0.29	74	Fe^0
		1.08	2.16		1.25	9	Fe^{2+}
		0.64	0.84		0.59	17	Fe^{3+}
300 (0–21 h)	823	0.26	0.00	331	0.28	95	Fe^0
		0.61	0.82		0.37	5	Fe^{3+}

doublet. These contributions can be assigned to two different divalent iron species (having isomer shifts of 0.98 and 0.75 mm/s) and an iron carbide (having an isomer shift of 0.21 mm/s). Most likely this iron carbide is θ-Fe_3C as is analogously seen for the unpromoted Fe/ZrO_2 (compare the parameters of θ-Fe_3C in Table 1 and the parameters of Fe_xC in Table 3). As mentioned previously, in order to avoid re-oxidation of the reduced catalyst, the catalyst is not cooled to room temperature. It is therefore not possible to verify the formation of θ-Fe_3C from its value of H_{eff} at 300 K.

Raising the reduction temperature to 623 K initially does not result in different spectral contributions. Measuring the catalyst, however, during a second 24 h leads to the appearance of a relatively low amount (1%) of metallic iron (Fe^0). During reduction at 653 K

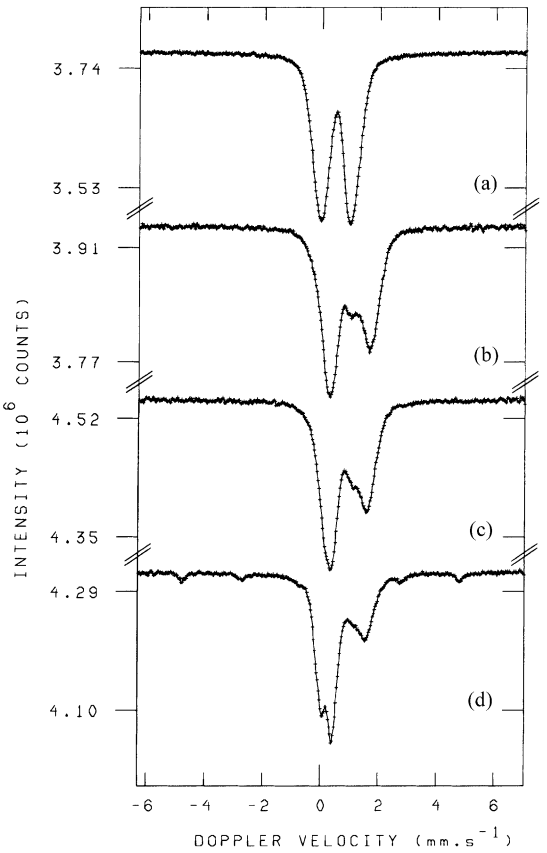

Fig. 7. Mössbauer spectra measured during reduction of $Fe/K/ZrO_2$ at ambient hydrogen pressure and at (a) 473 K, (b) 573 K, (c) 623 K, and (d) 653 K.

the spectral contribution of this Fe^0 increases only slightly and does not exceed 6%, however, the spectral contribution of the iron carbide increases with the reduction temperature up to a value of 40% at 653 K. This amount is twice as large compared to the amount formed during reduction of the unpromoted Fe/ZrO_2.

The low fraction of metallic iron formed during reduction seems to be related to the relatively large amount of carbon present after calcination. It is very likely that as soon as metallic iron is formed, it will take up carbon from the carbon deposits instantly forming an iron carbide. The rate of carburisation must be high. These results indicate that the iron species are initially reduced to metallic iron to a large extent. Throughout the reduction the two contributions related to divalent iron species diminish, but remain still present in relatively large amounts.

4. Discussion

4.1. Reduction and reduction model of Fe/ZrO_2 and $Fe/K/ZrO_2$

First of all, it is important to note that it is reported previously [12] that the calcination temperature of the support loaded with ammonium iron(III) citrate is not sufficiently high to completely remove the carbon species remaining after decomposition of the chelating citrate. As a result the zirconia support is covered by an amorphous layer containing iron(III) oxide and carbonaceous material.

Reduction at relatively low temperatures and ambient hydrogen pressure leads to the formation of two types of iron(II) species. From the observed TPR-profile and the absence of the two hyperfine splittings of magnetite in the measured Mössbauer spectra it is concluded that Fe_3O_4 is not an intermediate phase during the reduction to metallic iron. In addition, the Mössbauer measurements reveal the presence of high spin Fe^{2+} species with quadrupole splittings at room temperature (2.7–1.7 mm/s) significantly higher than for bulk FeO (about 0.55 mm/s). These results point to the formation of ferrous species due to an intimate interaction with the support [9–11,13–15,18,20–24]. One of the two iron(II) species is identified as a Fe^{2+} which upon formation immediately migrates into the zirconia support to form a mixed oxide. This species consists of fully coordinated iron(II) sites with the largest Q.S. value (Q.S. = 2.7 mm/s at T = 300 K). Chen et al. [11] studied the reduction of a 7 wt.% Fe_2O_3/ZrO_2 catalyst and claimed the presence of two different mixed oxides, viz., an initially formed spinel $(Zr_yFe_{3-y})O_4$, which subsequent transforms into $(ZrO_2)(FeO)_2$. Both oxides would appear in different reduction steps. Our experiments exclude such a transformation. Ghigna et al. [30] studied the incorporation of iron into a cubic ZrO_2 using Mössbauer spectroscopy, Fe K edge X-ray absorption spectroscopy and XANES. They found that iron enters the ZrO_2 lattice mainly as Fe^{2+} into two different sites, viz., interstitial sites and substitutionally into defect sites. The quadrupole splittings at room temperature are reported

Table 3
Mössbauer parameters of 2.5 wt.% Fe/K/ZrO_2 calculated from spectra measured during the reduction in H_2 at different temperatures

T (K)	I.S. (mm/s)	Q.S. (mm/s)	H_{eff} (kOe)	Γ (mm/s)	S.C. (%)	Compound
300 (0–20 h)	0.61	0.93		0.55	100	Fe^{3+}
373 (0–19 h)	0.55	1.02		0.57	100	Fe^{3+}
473 (0–22 h)	0.48	1.08		0.60	100	Fe^{3+}
573 (0–23 h)	0.75	0.71		0.61	30	Fe^{2+}
	0.98	1.47		0.61	66	Fe^{2+}
	0.21	0.55		0.30	4	Fe_xC
623 (0–26 h)	0.77	0.72		0.53	28	Fe^{2+}
	0.93	1.38		0.58	61	Fe^{2+}
	0.24	0.44		0.34	11	Fe_xC
623 (26–50 h)	0.00		295	0.34	1	Fe^0
	0.82	0.68		0.54	24	Fe^{2+}
	0.93	1.39		0.57	54	Fe^{2+}
	0.22	0.42		0.35	21	Fe_xC
653 (1–20 h)	0.00		295	0.29	3	Fe^0
	0.83	0.71		0.54	21	Fe^{2+}
	0.92	1.35		0.56	45	Fe^{2+}
	0.20	0.43		0.36	31	Fe_xC
653 (20–44 h)	0.03		296	0.29	4	Fe^0
	0.84	0.68		0.50	18	Fe^{2+}
	0.92	1.35		0.55	42	Fe^{2+}
	0.20	0.43		0.36	36	Fe_xC
653 (44–71 h)	0.02		297	0.27	4	Fe^0
	0.85	0.67		0.47	15	Fe^{2+}
	0.92	1.34		0.56	41	Fe^{2+}
	0.20	0.44		0.37	40	Fe_xC
653 (71–94 h)	0.02		298	0.27	6	Fe^0
	0.86	0.67		0.46	14	Fe^{2+}
	0.92	1.35		0.56	40	Fe^{2+}
	0.20	0.44		0.36	40	Fe_xC

to be for the two sites 2.41±0.07 and 2.04±0.03 mm/s (without assigning these contributions).

The second type of iron(II) species with the lowest Q.S. values most probably relates to a surface species on top of the mixed oxide having an unsaturated coordination. This species is assumed to be in contact with the carbon species present. It is likely that first the surface species is reduced to metallic iron. As mentioned, carbon is located in the proximity of the surface species, which appears to react with metallic iron. In this way, θ-Fe_3C is formed, which is observed to be present in relatively large particles (considering the sextuplet at 300 K). As only the carbide is observed at low reduction temperatures, the conversion of the metallic Fe^0 into a Fe-carbide proceeds relatively fast.

With increasing reduction temperature more and more metallic iron will be formed which directly reacts with the present carbon untill all carbon is used. Meanwhile carbon is removed out of the sample by hydrogenation to methane. As soon as all available carbon is transformed into θ-Fe_3C, metallic iron appears in the catalyst. The observed sextuplet at 300 K after reduction at 673 K and higher temperatures points to the presence of relatively large metallic iron particles. Ruckenstein and coworkers [31,32] claim that a zerovalent metal phase exhibits a higher interfacial free energy than the oxidic phase. The lower wettability of the oxidic support by metallic iron thus causes coalescence of Fe^0 resulting in the formation of large(r) particles. The sintering of metallic nickel particles was

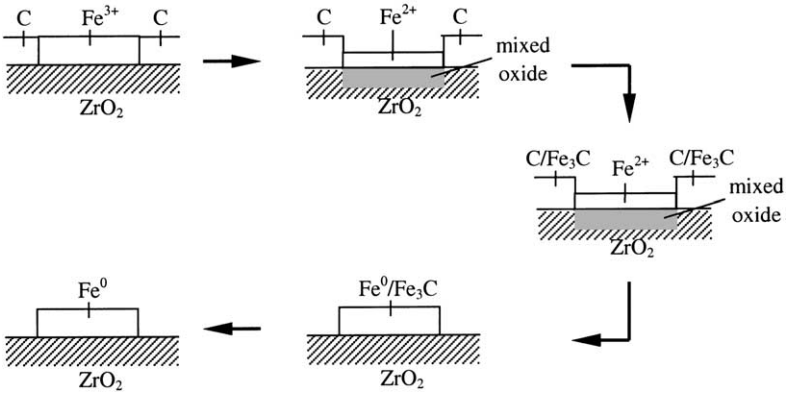

Fig. 8. Schematic model for the reduction of 2.5 wt.% Fe/ZrO_2. The sequence of reduction is indicated by the arrows.

found to proceed faster on a continuous $NiAl_2O_4$ layer [33]. However, in the catalyst under study, it is not likely that the low iron loading of our catalysts is sufficient to maintain a continuous layer of iron(II) oxide, but relatively large islands of iron are likely to exist. Coalescence of the metallic iron particles as indicated by the Mössbauer spectra can be understood in this way.

Co-impregnation with potassium carbonate changes the behaviour of the zirconia-supported iron catalysts. In the present study, it is shown that the potassium-rich sample reduces more easily at ambient pressure compared to the unpromoted catalyst. In literature, it is often encountered that potassium retards the reduction process by impeding the dissociation of hydrogen [34] or by blocking of the pores by potassium compounds limiting H_2 accessibility or preventing water to leave the reduced iron site. However, it is also reported that potassium—when part of the metal lattice—is able to enhance the hydrogen dissociation and, hence, the reduction [35]. The high initial dispersion of the catalysts in the present study may account for the enhanced reduction as was also observed by Guglielminotti et al. [36]. It is empirically established that upon mixing ammonium iron(III) citrate with potassium carbonate, NH_3 and CO_2 evolve, indicating that (at least part of the) potassium is atomically spread in the citrate precursor. Considering this, it is likely that the potassium species is well spread over the oxidic iron surface. Therefore, it may accelerate the dissociation of hydrogen on the iron surface and it will be so well spread that this compound does not block any pores (enabling water to be removed and hydrogen to be provided).

Based on the above, a model for the reduction of the iron(III) oxide supported by ZrO_2 is proposed. A schematic representation of this reduction model is shown in Fig. 8. A specific reduction temperature cannot be mentioned in the model as this temperature heavily depends on the amount of water present (or produced).

The initial state of the iron phase is characterised by a very thin (superparamagnetic) amorphous layer in which iron is exclusively in the trivalent state [12]. Upon reduction Fe^{3+} is converted to two Fe^{2+} species, one of which is related to a mixed oxide with a surface species on top of it. Reduction to metallic iron proceeds by the transformation of the surface species into metallic iron which reacts with the carbon to θ-Fe_3C. Subsequently an Fe^{2+} from the mixed oxide diffuses to the surface or has become a surface species. As soon as all available carbon in the sample is transformed into θ-Fe_3C and/or is hydrogenated to methane, rather large metallic iron particles or agglomerates are formed, which means a loss of dispersion. Finally, at a reduction temperature of 773 K or above even the carbon of the iron carbide is removed by hydrogenation to methane.

4.2. Re-oxidation in H_2 of reduced Fe/ZrO_2

The Mössbauer measurements have demonstrated that re-oxidation of the Fe^{2+} species formed in the catalyst during reduction at elevated temperatures

proceeds in hydrogen at ambient pressure upon cooling to 300 K. The quadrupole splitting of the trivalent iron species formed upon re-oxidation of the divalent species is not significantly different from that of the fresh calcined catalyst, which indicates that the number of surface ions has not changed upon reduction to Fe^{2+} and subsequent re-oxidation [37]. Hence, as to be expected, reduction to an iron oxide of a lower valency does not significantly affect its dispersion. A high water concentration within the support bodies causes oxidation to be thermodynamically feasible [17]. From the slow re-oxidation at 300 K of the Fe^{2+} species it can be concluded that transport of H_2O out of the pores of the support is very slow. Such a high residence time cannot be explained by diffusion alone, since water diffuses out of the pores within seconds [38]. Adsorption of water onto the pore walls or onto the iron surface is more likely to account for the slow transport. Agron et al. [39] have shown that monoclinic zirconia is capable of reacting with water to give two OH-groups at the support surface, or that water is physically adsorbed to a great extent. This was also observed on loaded zirconia [16]. Analogous to alumina [40], it is very likely that on zirconia two chemisorbed hydroxyl groups recombine to form water. This means that both chemisorbed and physisorbed H_2O may contribute to the slow removal of water out of the pores and, consequently, the re-oxidation of Fe^{2+}.

Re-oxidation of the formed iron-carbide phase (θ-Fe_3C) by water at low temperatures is not observed. This result can be explained as follows. The iron carbide phase is known to be very stable [41]. Severe oxidation of this phase by water at low temperatures is not expected. In addition, the Mössbauer spectra do not indicate the iron carbide particles to be extremely small, hence, oxidation of the surface of these particles will not be apparent from the Mössbauer spectra.

Also re-oxidation of the formed metallic Fe^0 particles is not observed during keeping the reduced Fe/ZrO_2 sample for different periods of time at room temperature. Molecular oxygen oxidises iron to a thickness of about 1.5 nm, but the extent of interaction of iron with water vapour has not been established accurately. Since water is observed to be much less reactive than molecular oxygen in the oxidation of iron [42], it is possible that the interaction with water vapour remains limited and leads to a coverage of about a monolayer of oxygen atoms and release of molecular hydrogen. If the reaction of water vapour with an iron surface covered by a monolayer of oxygen atoms does not proceed, the contribution of metallic iron to the spectra remains constant in time, as observed.

5. Conclusions

From the presented results it is deduced that the reduction of the initially present Fe^{3+} species at ambient pressure proceeds according to the steps shown in Fig. 9 for both catalysts Fe/ZrO_2 and $Fe/K/ZrO_2$.

In this figure, $Fe(I)^{2+}$ and $Fe(II)^{2+}$ denote surface and mixed oxide divalent iron species, respectively. Both species are directly formed upon reduction of Fe^{3+}, whereby this trivalent component is almost completely converted to Fe^{2+} before the metallic iron Fe^0 is formed. The mixed oxide species is stabilised by the support and is reduced at higher temperatures compared to the surface Fe^{2+} species.

As soon as metallic Fe^0 is present, θ-Fe_3C is immediately formed in both potassium-promoted and unpromoted catalysts. This formation is a consequence of the presence of carbon species remaining in both catalysts after decomposition of the organic chelate precursor. The amount of θ-Fe_3C is larger in the potassium-promoted catalyst. The above reduction process is found to proceed faster on the potassium-rich catalyst.

It is further shown that water (formed during reduction) can hardly be removed due to adsorption on

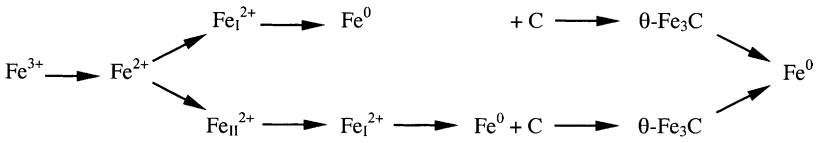

Fig. 9. Reduction of highly dispersed trivalent iron.

the pore walls of the support. This water gives rise to re-oxidation when the reaction temperature is decreased to 300 K. Remarkable is the observation that only Fe^{2+} is oxidised to Fe^{3+} and not Fe^{0}, which is explained by an oxidic protecting layer. In view of these considerations, it should be borne in mind that high local water concentrations may lead to misinterpretations of the iron species present in the initial stage during e.g. the Fischer–Tropsch reaction.

References

[1] F. Fischer, H. Tropsch, Brennstoff-Chem. 4 (1923) 276.
[2] F. Fischer, H. Tropsch, Brennstoff-Chem. 7 (1926) 97.
[3] F. Fischer, H. Tropsch, Brennstoff-Chem. 11 (1930) 489.
[4] F. van Looij, Ph.D. Thesis, Utrecht University, Utrecht, The Netherlands, 1994.
[5] V. Ponec, Adv. Catal. 32 (1983) 149.
[6] W. Teunissen, Ph.D. Thesis, Utrecht University, Utrecht, The Netherlands, 2000.
[7] P.H. de Bokx, A.J.H.M. Kock, E. Boellaard, E. Klop, J.W. Geus, J. Catal. 96 (1985) 468.
[8] L.A. Boot, A.J. van Dillen, J.W. Geus, F.R. van Buren, J. Catal. 163 (1996) 186.
[9] E. Guglielminotti, J. Phys. Chem. 98 (1994) 4884.
[10] E. Guglielminotti, J. Phys. Chem. 98 (1994) 9033.
[11] K. Chen, Y. Fan, Z. Hu, Q. Yan, Catal. Lett. 36 (1996) 130.
[12] F.R. van den Berg, M.W.J. Crajé, P.J. Kooyman, A.M. van der Kraan, J.W. Geus, Appl. Catal. A Gen. 235 (2002) 217.
[13] B.J. Tatarchuk, J.A. Dumesic, J. Catal. 70 (1981) 335.
[14] S.J. Tauster, S.C. Fung, R.T.K. Baker, J.A. Horsley, Science 211 (4487) (1981) 1121.
[15] D.E. Stobbe, F.R. van Buren, A.W. Stobbe-Kreemers, A.J. van Dillen, J.W. Geus, J. Chem. Soc., Faraday Trans. 87 (10) (1991) 1631.
[16] L.A. Boot, Ph.D. Thesis, Utrecht University, Utrecht, The Netherlands, 1994.
[17] A.J.H.M. Kock, H.M. Fortuin, J.W. Geus, J. Catal. 96 (1985) 261.
[18] X. Gao, J.Shen.Y. Hsia, Y. Chen, J. Chem. Soc. Faraday Trans. 89 (7) (1993) 1079.
[19] Gmelins Handbuch der Anorganische Chemie, 59: Eisen, Teil A-Ableihung II, Verlag Chemie, Berlin, Germany, 1692.
[20] M.V. Cagnoli, S.G. Marchetti, N.G. Gallegos, A.M. Alvarez, R.C. Mercader, A.A. Yeramian, J. Catal. 123 (1989) 21.
[21] A.F.H. Wielers, A.H.J.M. Kock, C.E.C.A. Hop, J.W. Geus, A.M. van der Kraan, J. Catal. 117 (1989) 1.
[22] Y.-Y. Huang, J.R. Anderson, J. Catal. 40 (1975) 143.
[23] M.C. Hobson Jr, H.M. Gager, J. Colloid Interface Sci. 34 (3) (1970) 357.
[24] S. Yuen, Y. Chen, J.E. Kubsh, J.A. Dumesic, N. Topsøe, H. Topsøe, J. Phys. Chem. 86 (1982) 3022.
[25] A.M. van der Kraan, J.W. Niemantsverdriet, In: G.J. Long, J.G. Stevens (Eds.), Industrial Applications of the Mössbauer Effect, Plenum Press, New York, 1986, p. 609.
[26] P.W. Selwood, Chemisorption and Magnetization, Academic Press, New York, 1975.
[27] G.B. Raupp, W.N. Delgass, J. Catal. 58 (1979) 348.
[28] J.W. Niemantsverdriet, Spectroscopy in Catalysis, VCH, Weinheim, 1993 (Chapter 5).
[29] O.J. Wimmers, P. Arnoldy, J.A. Moulijn, J. Phys. Chem. 90 (1986) 1331.
[30] P. Ghigna, G. Spinolo, U. Anselmi-Tamburini, F. Maglia, M. Dapiaggi, G. Spina, L. Cianchi, J. Am. Chem. Soc. 121 (1999) 301.
[31] I. Sushumna, E. Ruckenstein, J. Catal. 94 (1985) 239.
[32] E. Ruckenstein, X.D. Hu, J. Catal. 100 (1986) 1.
[33] P.H. Bolt, Ph.D. Thesis, Utrecht University, 1994 (Chapter 7).
[34] C.-K. Kuei, J.-F. Lee, M.-D. Lee, Chem. Eng. Comm. 101 (1991) 77.
[35] J.J. Mortenson, B. Hammer, J.K. Norskov, Phys. Rev. Lett. 80 (1998) 4333.
[36] E. Guglielminotti, F. Boccuzzi, F. Pinna, G. Strukul, J. Catal. 167 (1997) 153.
[37] A.M. van der Kraan, Phys. Stat. Sol. (a) 18 (1973) 215.
[38] J.H. de Boer, The Dynamical Character of Adsorption, Clarendon Press, Oxford, 1953.
[39] P.A. Agron, E.L. Fuller Jr, H.F. Holmes, J. Colloid Interface Sci. 52 (1975) 553.
[40] H. Knözinger, P. Ratnasamy, Catal. Rev. Sci. Eng. 17 (1978) 31.
[41] Thermodynamic calculations with “HSC Chemistry”, Version 3.02, Outukumpu Research oy, Pori, Finland.
[42] S.J. Roosendaal, Ph.D. Thesis, Utrecht University, Utrecht, The Netherlands, 1999 (Chapter 6).